J Fluoresc (2015) 25:1931–1949
DOI 10.1007/s10895-015-1685-z

ORIGINAL ARTICLE

Monitoring the Competence of a New Keto-tetrahydrocarbazole Based Fluorosensor Under Homogeneous, Micro-Heterogeneous and Serum Albumin Environments

Amrit Krishna Mitra[1] · **Abhishek Sau**[2] · **Subhas Chandra Bera**[2] · **Suchandra Chakraborty**[3] · **Chandan Saha**[3] · **Samita Basu**[2]

Received: 29 July 2015 / Accepted: 28 September 2015 / Published online: 21 October 2015

Abstract We present here a detailed photophysical study of a recently synthesised fluorophore 8-methyl-8,9-dihydro-5H-[1,3]dioxolo[4,5-b]carbazol-6(7H)-one. This is a synthetic precursor of bio-active carbazole skeleton Clausenalene. Spectroscopic investigation of the fluorophore has been carried out in different protic and aprotic solvents, as well as in binary solvent mixtures, using absorption, steady-state and time-resolved fluorescence techniques. This fluorophore is particularly responsive to the hydrogen bonding nature as well as polarity of the solvent molecules. When considered in micelles and β-cyclodextrin, this behaves as a reporter of its immediate microenvironment. Steady state and time resolved fluorometric and circular dichroism techniques have been used to explore the binding interaction of the fluorophore with transport proteins, bovine serum albumin and human serum albumin. The probable binding sites of the fluorophore in the proteinous environments have been evaluated from fluorescence resonance energy transfer study. Laser flash photolysis experiments also have been performed to observe the triplet excited state interaction between the fluorophore and albumin proteins.

Keywords Keto-tetrahydrocarbazole · Micelles · Micro-heterogeneity · Laser flash photolysis · Serum albumin · FRET

Electronic supplementary material The online version of this article (doi:10.1007/s10895-015-1685-z) contains supplementary material, which is available to authorized users.

✉ Samita Basu
samita.basu@saha.ac.in

[1] Department of Chemistry, Government General Degree College, Singur, Hooghly, West Bengal 712409, India

[2] Chemical Sciences Division, Saha Institute of Nuclear Physics, Kolkata 700064, India

[3] Department of Clinical and Experimental Pharmacology, School of Tropical Medicine, Kolkata 700073, India

Introduction

For the last few decades, fluorescent carbazole derivatives, due to their reputable spectral properties, have found application in various areas like light emitting diodes, potential photosensitive biological units, fluorescent markers in biology, photo-induced electron sensors and in diverse fields of chemistry (photoelectrical dyes, supramolecular recognitions and medicinal chemistry) [1]. Increasing attention has been paid to this skeleton as it owns appropriate electronic and charge transport properties, as well as a large π-conjugated system [1–4] (http://en.wikipedia.org/wiki/carbazole). Several sophisticated approaches [5] have been developed for the syntheses of carbazole derivatives but one of the classical methods involves the synthesis of keto-tetrahydrocarbazole derivatives and then functional group interconversion to obtain the said skeleton [6–8]. Expedition on this route reveals that methoxy and methylenedioxy derivatives of keto-tetrahydrocarbazole show fluorescence and act as reporters of their immediate environment [6, 9–13]. Such small organic fluorescent probes are always important as they can be used as labelling agents and sensors in both chemical and biological systems [14]. Here, we are introducing detailed solution phase photophysics of a recently synthesised fluorophore 8-methyl-8,9-dihydro-5H-[1,3]dioxolo[4,5-b]carbazol-6(7H)-one (MTDCO) [6]. MTDCO is a synthetic precursor of bio-active carbazole skeleton Clausenalene (Scheme 1). Bhattacharyya et al. in the year 1993 isolated Clausenalene [7] from the benzene extract of stem bark of *Clausena*

Scheme 1 Representative structure of MTDCO and Clausenalene

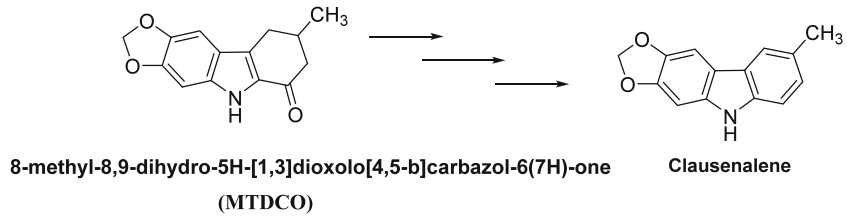

8-methyl-8,9-dihydro-5H-[1,3]dioxolo[4,5-b]carbazol-6(7H)-one (MTDCO)

Clausenalene

heptaphylla, the first methylenedioxy based carbazole alkaloid from a plant source. Rashid et al., in the year 2001, reported [8] antibacterial activity of *Clausena heptaphylla.* It was found to have anti-bacterial activity again both Gram-positive and Gram-negative bacteria. Later on, Clausenalene has been synthetically prepared using MTDCO as an important synthetic intermediate [7, 8]. So we have paid interest on MTDCO to forecast its probable biological activities through fundamental spectroscopic techniques.

Initially, we have studied solvent effects on this fluorophore in order to predict the fundamental solvation dynamics to estimate the enhancement of electric dipole moment of molecules in the excited states, hydrogen-bond interactions, assessing the micro-environmental features of biochemical systems and many others. In continuation of this study, we have also monitored the spectral responses of MTDCO in a mixture of two solvents as it is more complicated as compared to a pure solvent. Apparently, the binary mixtures are macroscopically homogeneous; nevertheless, they form small clusters resulting from differential H-bonding, hydrophobic and dipole-dipole interactions [15]. Monitoring the fluorescence sensing competence of MTDCO with a slight variation of environment, we have paid interest to the effect of microheterogeneity on MTDCO in the form of different micelles [anionic (sodium dodecyl sulfate) SDS, non-ionic (Triton X-100) TX-100 and cationic (cetyltrimethylammonium bromide) CTAB] and β-cyclodextrin (β-CD). Photophysical studies in constrained micellar environments are important due to their ability of mimicking biological systems [16–24]. β-cyclodextrin is generally considered as a nano-vessel [25] as it has the potentiality to embed appropriately sized molecules and the resulting supramolecules [26] can serve as models for enzyme–substrate complexes [26–28]. Motivated by the spectral possessions of MTDCO in different microheterogeneous environments, we have inspected the interaction between MTDCO and most widely studied transport proteins, human serum albumin (HSA) and bovine serum albumin (BSA) [29, 30] since the engineering of protein-small molecule interaction is becoming essential nowadays to recognize the crucial biochemical processes in living systems. Serum albumins are the most abundant proteins in plasma [31]; they contribute to colloid osmotic blood pressure and are essentially responsible for the maintenance of blood pH [32]. They can play a dominant role in drug disposition [33] and efficacy [34]. The solubility of hydrophobic drugs in plasma is increased by serum albumins and their delivery to cell is regulated in vivo. Bovine and human serum albumins show around 80 % sequence homology and a repeating pattern of disulfides [35]. One of the main differences between the two proteins is that BSA has two tryptophan residues (Trp-134 and Trp-212) and HSA, only one (Trp-214) [36]. The presence of two major binding sites, viz., Sudlow's sites I and II are chiefly accountable for the specific delivery of drugs by serum albumins [37]. At site I, the binding affinity is primarily governed by hydrophobic interaction, whereas, in site II, all the processes like hydrophobic, hydrogen bonding and electrostatic interactions occur [38]. There may be certain molecules that show preferential binding at site II and have higher affinity for serum albumins. Such molecules exhibit efficient photodynamic therapeutic applications [36–38]. Many drugs and other bioactive small molecules bind reversibly to albumin which implicates their role as carriers. Consequently, it is important to study the interactions of drugs with this protein.

Methoxy and methylene-dioxy derivatives of Keto-tetrahydrocarbazole form a class of compounds whose absorption and emission characteristics are strongly dependent on their environments [9–13]. Hence, they are used to study solvation interactions in homogeneous and microheterogeneous media. Thus, the spectroscopic and photophysical study of these molecular systems in serum albumin media is very helpful for a better understanding of the nature of binding and biodistribution inside the living cells although no one has ever made any foray into it before this.

Experimental Section

UV Spectroscopic grade benzene (Bz), toluene (Tol), 1,4-dioxane (DOX), ethyl acetate (EtAc), tetrahydrofuran (THF), acetonitrile (ACN), dimethyl formamide (DMF), dimethyl sulphoxide (DMSO), water (H_2O), ethanol (EtOH), methanol (MeOH) and butanol (BuOH) have been purchased from Spectrochem Pvt. Ltd. and used in their original forms. AR grade hexanol (HxOH), octanol (OcOH), decanol (DcOH) and dodecanol (DdOH) have been purchased from Loba Chemie Pvt. Ltd. and used after several proper distillation processes. We have used anhydrous solvents for our spectroscopic perusal. To check the purity level of the solvent, we have used steady

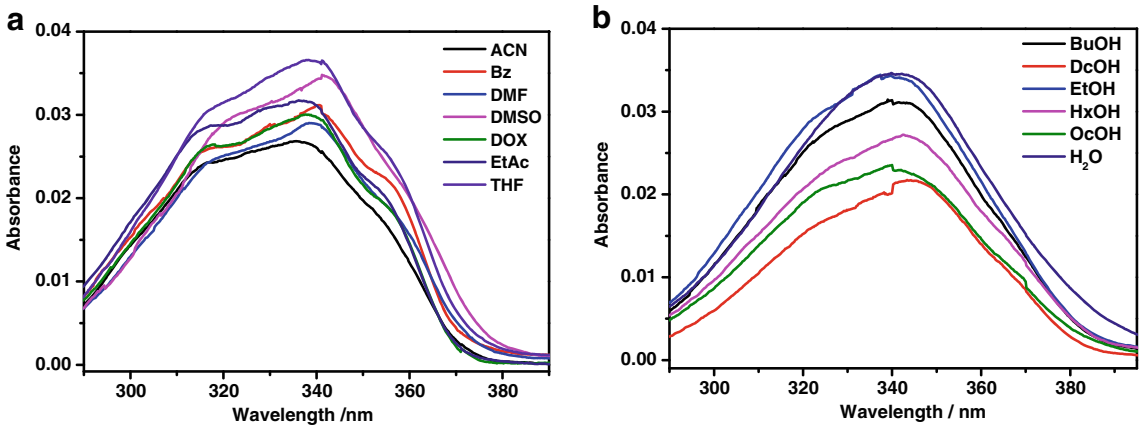

Fig. 1 Absorption spectra of MTDCO **a** aprotic solvents and **b** protic solvents. Concentration of the compound is 1×10^{-6} M

state and time-resolved fluorescence experiments in the wavelength ranges of interest. BSA and HSA have been obtained from SRL. We have purchased anthracene from Sigma-Aldrich and have used it after recrystallization. Water from Milipore water purification system has been used. Jasco V-650 spectrophotometer and Horiba Jobin-Yvon Fluoromax-3 have been used for absorbance and fluorescence measurements respectively. Fluorescence lifetimes have been measured using a time-correlated single-photon-counting (TCSPC) spectrophotometer (Horiba Jobin-Yvon Single Photon Counting Controller Fluorohub). The sample has been excited at 340 nm using an LED. The fluorescence quantum yield (Φ_F) is measured with reference to anthracene by comparing the area of fluorescence and absorbance at the excitation wavelength, using the formula [1]

$$\Phi_F = \Phi_R \frac{I_F}{I_R} \times \frac{O.D_R}{O.D_F} \times \left(\frac{\eta_F}{\eta_R}\right)^2 \quad (1)$$

where Φ is the quantum yield, I is the integrated fluorescence intensity, OD is the optical density and n is the refractive index. The subscripts R and F refer to the reference fluorophore anthracene and MTDCO respectively. For a given sample, the wavelength at which absorbance is the maximum (λ_{max}) is used as the excitation wavelength for the corresponding emission scan. The lifetime is obtained using deconvolution technique which is based on a convolution integral. We have used IBH DAS 6.2 data analysis software in which reduced χ^2 and weighted residuals serve as parameters for goodness of fit. All the steady-state and time-resolved measurements have been performed with a temperature stabilization. Nanosecond flash photolysis set-up (Applied

Table 1 Absorption maxima ($\lambda_{abs/nm}$), emission maxima ($\lambda_{fl/nm}$), quantum yield (ϕ_f), fluorescence lifetime (τ), radiative decay constant (k_r) and non-radiative decay constant (k_{nr}) of MTDCO in different solvents

Solvents	$\lambda_{abs\ /nm}$	$\lambda_{fl\ /nm}$	ϕ_f	a_1 (a_2)	τ_1 (τ_2)/ ns	τ_{av}/ ns	χ^2	$k_r\times10^{-7}$ / s^{-1}	$k_{nr}\times10^{-7}$ / s^{-1}
BZ	337	383	0.032	1	0.380	0.380	1.17	8.42	254.73
DOX	337	392	0.048	1	0.392	0.392	1.15	12.24	242.85
EtAc	338	393	0.052	1	0.364	0.364	1.16	14.28	260.43
DMF	337	401	0.182	1	1.088	1.088	0.98	16.72	75.18
ACN	336	403	0.289	1	1.834	1.834	1.06	27.94	68.76
DMSO	341	407	0.316	1	1.675	1.675	0.99	18.86	40.83
THF	340	407	0.047	1	0.591	0.591	1.18	7.95	161.25
DcOH	340	423	0.089	0.32 (0.68)	0.340 (1.089)	0.850	1.05	10.47	107.17
BuOH	341	430	0.076	1	1.087	1.087	1.05	6.99	85.00
OcOH	343	432	0.077	0.28 (0.72)	0.245 (1.014)	0.798	1.17	9.64	115.66
HxOH	342	435	0.088	0.21 (0.79)	0.226 (0.943)	0.792	0.99	11.11	115.15
EtOH	342	436	0.066	1	1.318	1.318	1.02	5.00	70.86
H_2O	341	467	0.143	1	2.574	2.574	0.99	5.55	33.29

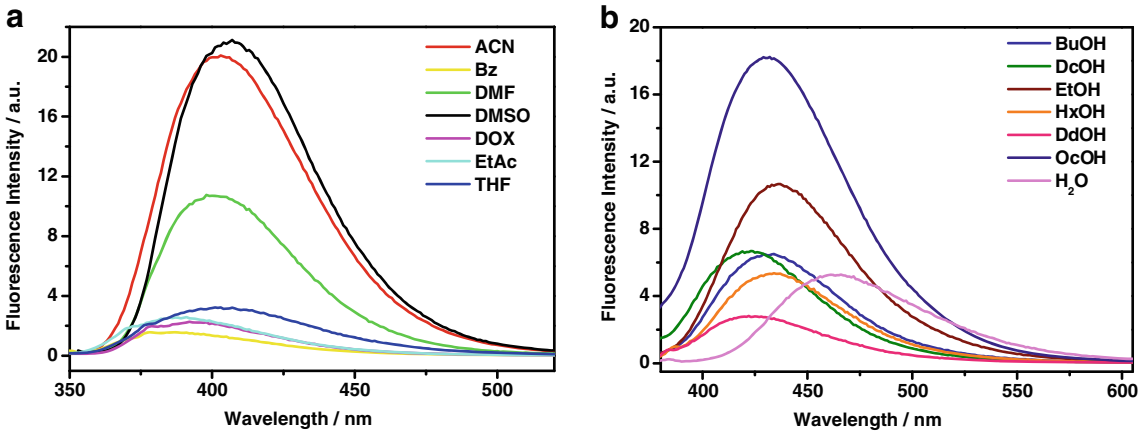

Fig. 2 Fluorescence emission spectra of MTDCO **a** aprotic solvents **b** protic solvents. Concentration of the compound is 1×10^{-6} M. Emission spectra have been taken exciting the samples at their corresponding absorption maxima

Photophysics) containing Nd:YAG (Lab series, Model Lab 150, Spectra Physics) laser has been used for the measurement of transient absorption spectra. The sample has been excited at 355 nm (FWHM=8 ns) using Nd-YAG laser (Lab series, Model Lab 150, Spectra Physics). Transient species in solution have been monitored through absorption of light from a pulsed xenon lamp (150 W) at right angle to the laser beam. The wavelength from the probe beam is dispersed with a monochromator and detected with R928 photomultiplier detector. The photomultiplier output is fed into a 600 MHz, 4 Gs/s, DSO8064A Agilent Infiniium oscilloscope and the data are transferred to Laser software running in an Iyonix range of ARM-based RISC OS computer. The samples are de-aerated for 20 min by passing pure argon gas prior to each experiment. All the data have been analysed fitted and plotted by the software Origin® 8.0 Pro. All experiments have been carried out using quartz cuvettes of 1 cm^2 cross-sections purchased from Hellma Analytics. Phosphate buffer solution (pH~7 and ionic strength=0.15 M) has been used as the buffer solution. Synthesis and crystallization of MTDCO have been performed as described elsewhere [6].

Results and Discussions

Behaviour of MTDCO in Different Pure Homogeneous Solvents

Figure 1a and b show absorption spectra of MTDCO in different solvents, both protic and aprotic, with varied dielectric constants. The spectroscopic and photophysical properties of MTDCO in homogeneous solvents are collected in Table 1. In all aprotic solvents studied, transition is located in a narrow wavelength range, between ~336 nm to ~339 nm and in protic solvents ~342 nm. Therefore, the absorption spectra are hardly solvent dependent. High molar absorption coefficients (~10^5) indicate π to π* transition in all the solvents. Fluorescence quantum yields of the compounds have been calculated with anthracene as the reference fluorophore (Table 1). Standard procedure is followed to calculate the value of the quantum yields.

Emission profile (Fig. 2a and b) of MTDCO is far more sensitive than its corresponding absorption spectra with respect to both polarity and protic nature of the solvents.

As we move from Bz (~383 nm) to H_2O (~467 nm) significant bathochromic shift is observed. It is worthwhile to mention, while moving along the series of protic solvents DcOH (~423 nm) to H_2O (~467 nm) via BuOH (~430 nm), HxOH (~435 nm) and EtOH (~436 nm), systematic red shift is noticed with increase in dielectric constant, empirical polarity parameter (E_T30) and hydrogen bond donor (HBD) acidity of the solvent (solvent

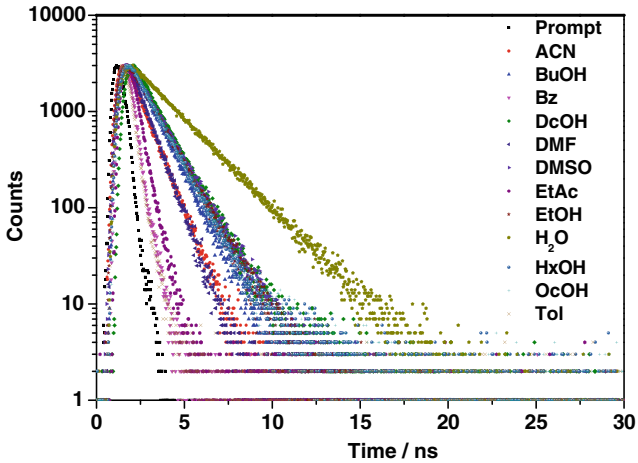

Fig. 3 Fluorescence lifetime decays of MTDCO in different solvents. Concentration of the compound is 1×10^{-6} M. MTDCO is excited using a 340 nm LED

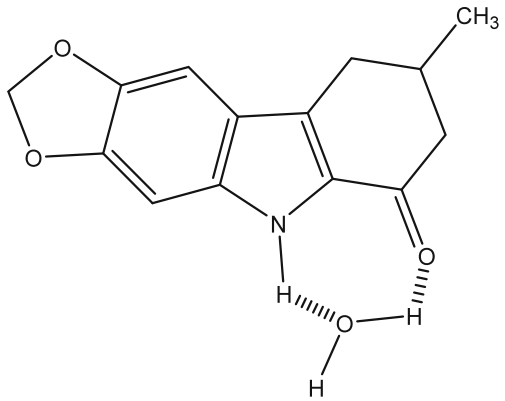

Scheme 2 Structure of hydrogen bonded MTDCO in water

parameters are given in Supporting Information S1). Closer scrutiny of the emission spectra in the case of aprotic solvents indicates that significant intensity enhancement is found in case of solvents having high dielectric constant. The polarity-dependence of the red shift observed in the emission spectra is very prominent compared to that in the absorption spectra indicating that polar solvents stabilize the excited state [1]. Solvent relaxation is mainly responsible for the observed red shift. During relaxation, polar solvents reorient themselves to minimize the energy of the system in response to changes in the electrical properties of MTDCO due to excitation. This polarity dependent red shift observed in fluorescence emission shows a distinct difference between the Frank-Condon S1 state and the solvent relaxed S$^{'}$1 state in various solvents [1]. Reasonable fluorescence quantum yields are obtained in all the solvents used. It is found to be maximum in polar aprotic solvents like DMSO (0.316), ACN (0.289) and DMF (0.182). Non-radiative decay constant is lesser in these solvents. Fluorescence decay profiles of MTDCO in different solvents have been shown in Fig. 3. Corresponding decay parameters have been calculated using Eq. (2) and are listed in Table 1.

$$I(t) = \sum_{i=1}^{n} a_i e_i^{-t/\tau_i} \tag{2}$$

I(t) represents fluorescence intensity at time t, a_i is the pre-exponential factor for the fluorescence intensity, τ_i is the fluorescence lifetime of the emitting species and n is the total number of emitting species. We have followed relations (3) and (4) to calculate the radiative (k_r) and non-radiative (k_{nr})

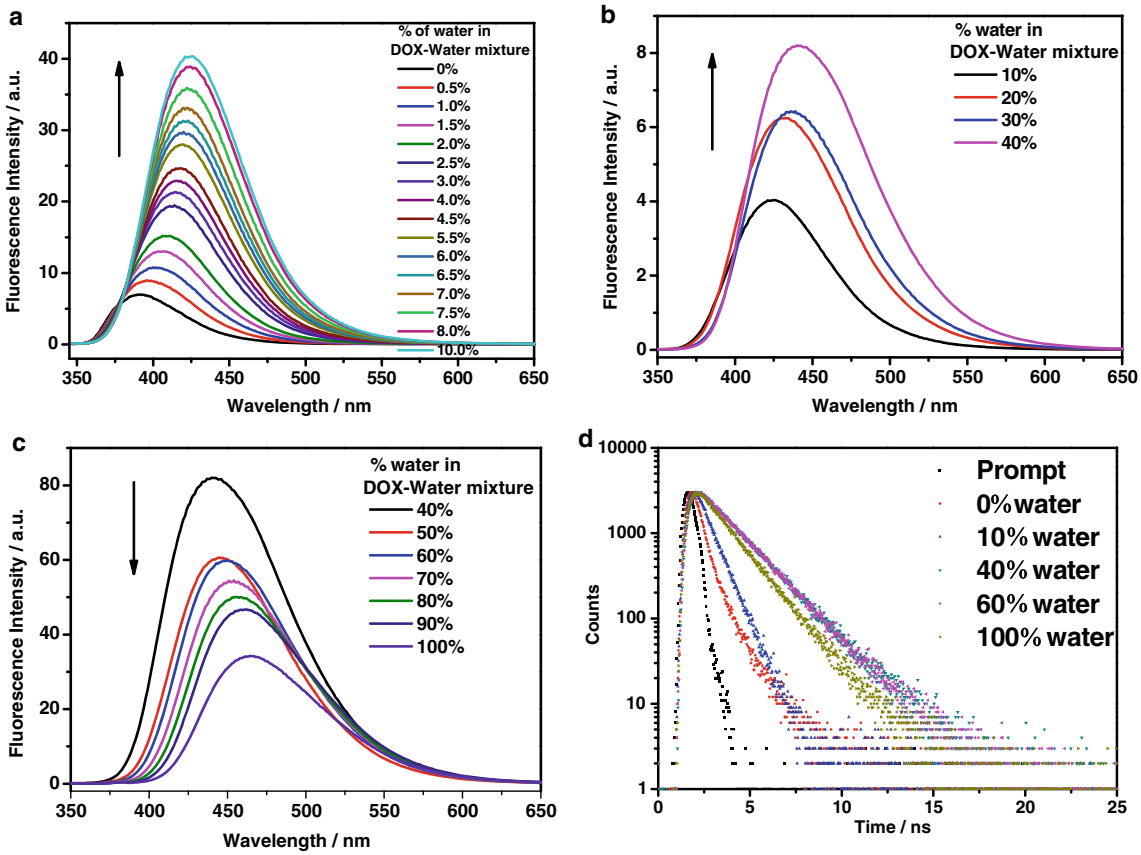

Fig. 4 Fluorescence emission spectra of MTDCO with the variation of %water in DOX-Water system (**a-c**). Fluorescence lifetime decays of MTDCO (excited using a 340 nm LED) in different compositions of dioxane-water mixtures (**d**). Concentration of the compound is 1×10^{-6} M. Emission spectra have been taken exciting the samples at their corresponding absorption maxima

decay rates of MTDCO in different environments and the values are listed in Table 1.

$$k_r = \frac{\phi_f}{\tau_f} \tag{3}$$

$$k_{nr} = \frac{(1-\phi_f)}{\tau_f} \tag{4}$$

Fluorescence quantum yields and lifetimes of MTDCO in a specific medium have been represented by ϕ_f and τ_f respectively. In case of bi-exponential decays, we have used average lifetimes [1] (amplitude weighted) to calculate the radiative and non-radiative decay rates.

Quantum yield and lifetime of MTDCO generally increase in the aprotic solvents as the $E_T(30)$ value of the solvent increases. However, no such trend, depending on a particular solvent parameter, is observed in the case of protic solvents. When it comes to long chain alcohols, fluorescence decay profiles are better fitted in a bi-exponential decay equation as MTDCO is differentially solvated to polar head groups and the hydrophobic tail regions of such alcohols [10].

We have observed a substantial drop in fluorescent quantum yield as we move from ACN (0.289), DMSO (0.316), DMF (0.182) to different alcoholic solvents (0.06–0.08); however, quantum yield is considerably recovered in water (0.143). Lifetime (τ~2.57) of MTDCO in water is maximum among all the solvents. Empirical polarity parameter (E_T30), dielectric constant, π^* value (representative of polarity/polarizability of the solvent), α value (representative of hydrogen bond donor acidity), solvent dipolarity and solvent acidity values of water are maximum compared to other solvents (solvent parameters are given in Supporting Information S1) and these parameters surely have something to play with the excited state affairs of MTDCO in water. The radiative transitions and the relaxation dynamics of MTDCO in the excited state can be explained by its solvent-specific H-bonding interaction after photoexcitation. Zhao et al. in a number of recent works have emphasized the formation and dynamics of excited state H-bonding and its significance in facilitating the radiationless deactivation pathways of photoexcited carbonyl chromophores [39, 40]. They have reported a decrease in lifetime of the chromophores due to opening of some nonradiative channels in polar H-bond donating solvents and have assigned this behaviour to some specific H-bonding interactions between the chromophore and solvent. We have observed similar photophysical properties of MTDCO, as

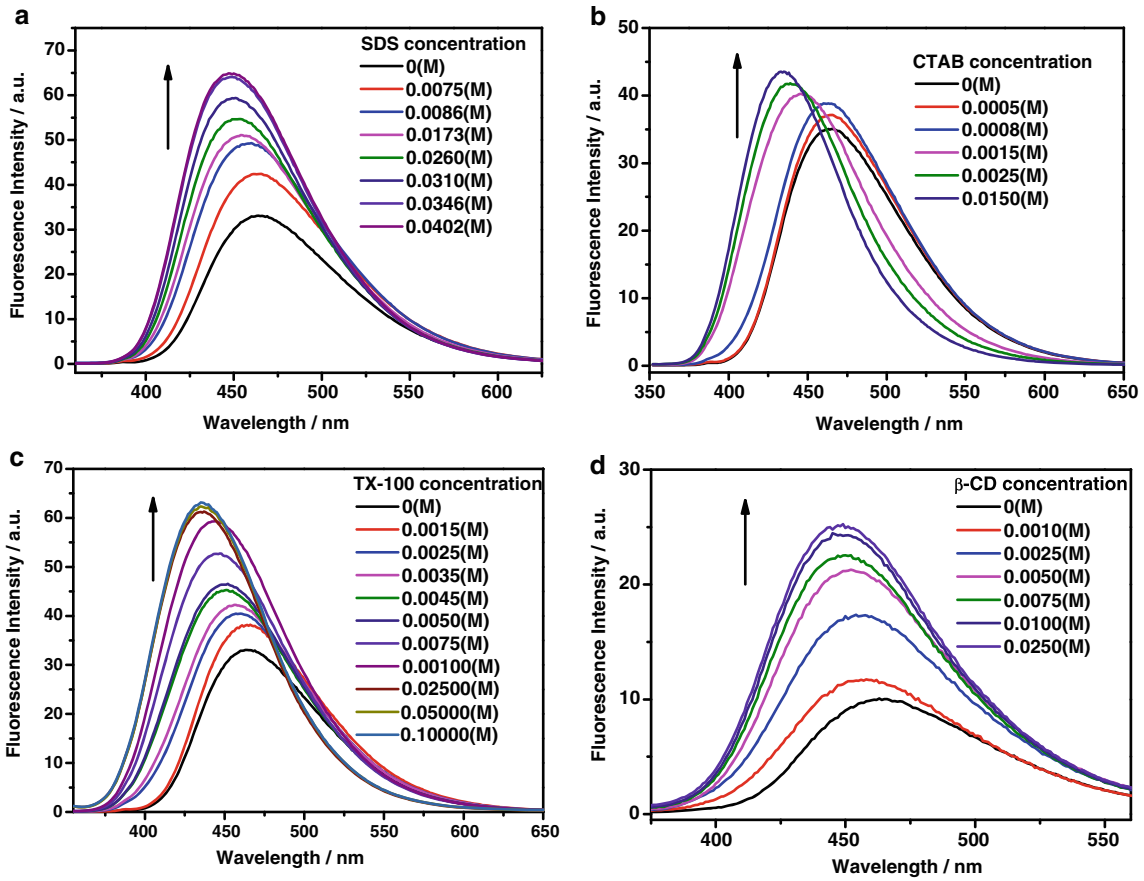

Fig. 5 Fluorescence emission spectra (**a**,**b**,**c**,**d**) of MTDCO in aqueous SDS, CTAB, TX-100 and β-CD solutions respectively. Concentration of the compound is 1×10^{-6} M. Emission spectra have been taken exciting the samples at their corresponding absorption maxima

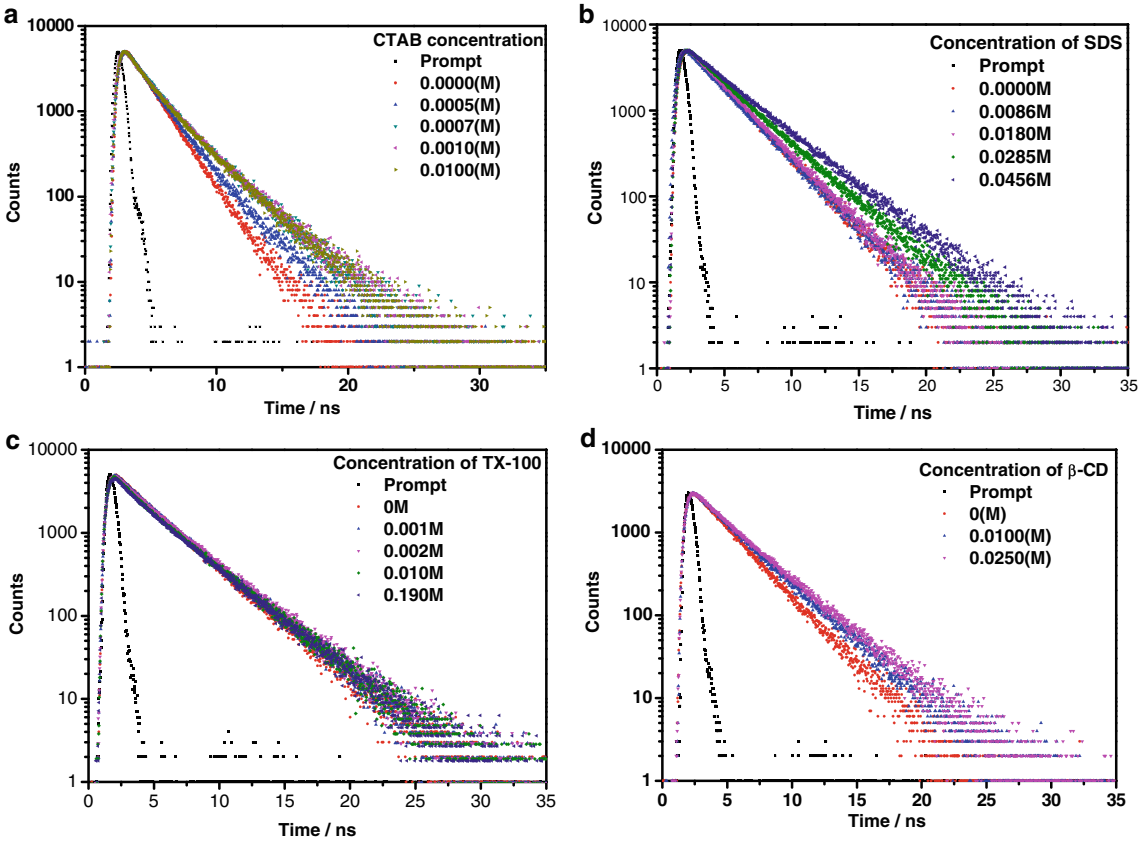

Fig. 6 **a** Fluorescence lifetime decays of MTDCO in **a** aqueous CTAB solutions **b** aqueous SDS solutions **c** aqueous Tx-100 solutions **d** aqueous β-CD solutions. Concentration of the compound is 1×10^{-6} M. (corresponding decay parameters are outlined in Supporting Information S7). MTDCO is excited using a 340 nm LED

we move from ACN, DMSO and DMF to alcoholic solvents. However, as we move from alcoholic solvents to water, instead of a further decrease we have observed an enhancement of lifetime of MTDCO. This sort of photophysical behaviour of MTDCO is due to two different excited emitting states, (a) MTDCO and (b) hydrogen-bonded MTDCO (h-MTDCO). In non-aqueous medium, we have observed the fluorescence of MTDCO, which decreases with H-bonding environment of the solvent around MTDCO. However, in water, we observe the fluorescence from a separate isomer, h-MTDCO. On photoexcitation, the efficient and rigid H-bonding network in water favours formation of h-MTDCO due to statistical abundance of two O–H bonds; however, in nonaqueous solvent (even in alcohols) the formation of h-MTDCO is not that much favoured due to the lack of efficient H-bonding and steric hindrance of the alkyl group in forming a suitable H-bonded clathrate. On the contrary, the small but labile water molecules can easily form H-bonds between the N−H moiety

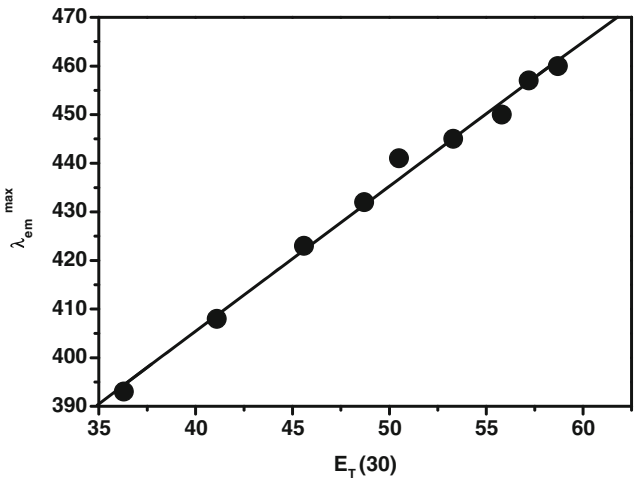

Fig. 7 Variation of the emission maximum of MTDCO (Concentration of the compound is 1×10^{-6} M) with $E_T(30)$ in dioxane–water mixtures

Table 2 Binding constants and free energy changes for MTDCO – micelle interaction

Nature of the micelle	Binding constant (K) in mol^{-1}	ΔG^0 /kJ mol^{-1}
SDS	104,646	−28.24
CTAB	173,611	−29.48
TX-100	512,321	−32.12

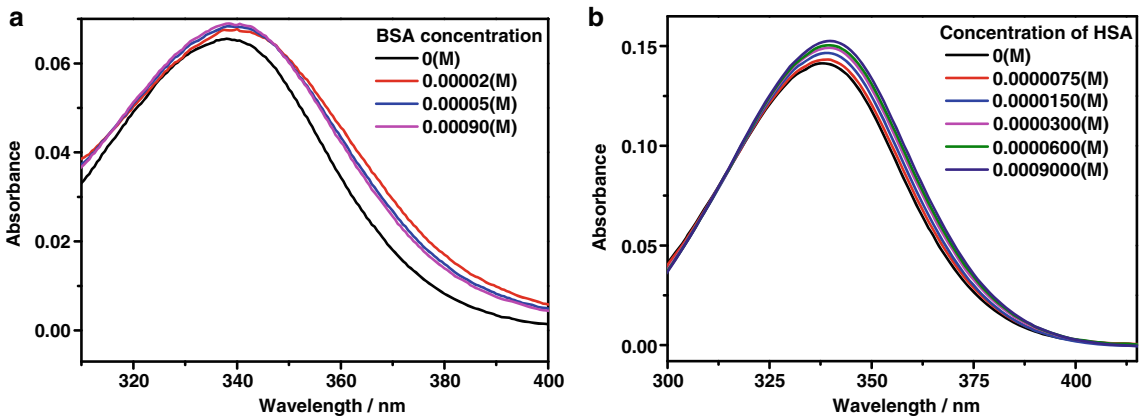

Fig. 8 Absorption spectra of MTDCO in the presence of different concentrations of **a** BSA and **b** HSA. Concentration of the compound is 1×10^{-6} M

and adjacent carbonyl oxygen of MTDCO, forming a H-bonded ring structure (Scheme 2). The strengthening of the H-bonds in its electronic excited states assists the formation of a rigid framework of H-bonded MTDCO in water, which greatly suppresses the rate of different nonradiative (k*nr*) processes resulting in higher fluorescence lifetime and quantum yield (compared to other protic solvents).

In the later portions of this manuscript, we have inspected the dependence of MTDCO on individual solvent parameters and have discussed the role of water in detail ("Effect of Binary Mixtures on the Excited State Affairs of MTDCO (Role of Water)" section). Now, monitoring the bathochromic shift in the emission spectrum of MTDCO with the increase in solvent polarity, we are interested to measure the enhancement

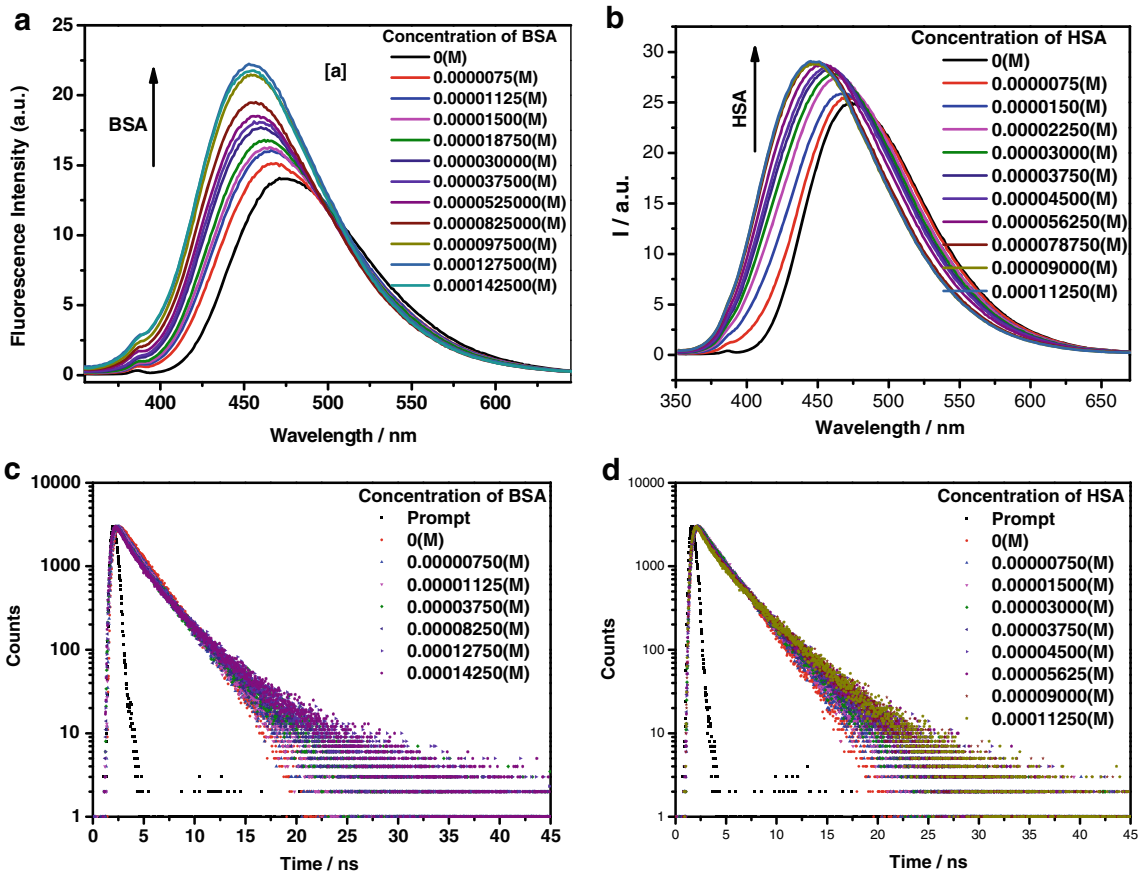

Fig. 9 Fluorescence emission spectra of MTDCO in the presence of different concentrations of BSA (**a**) and HSA (**b**). Emission spectra have been taken exciting the samples at their corresponding absorption maxima. Corresponding fluorescence lifetime plots of MTDCO (excited using a 340 nm LED) in presence of BSA (**c**) and HSA (**d**). Concentration of the compound is 1×10^{-6} M

of dipole moment in excited state [41, 42]. We have calculated the changes in dipole moment of MTDCO in both protic (11.02 D) and aprotic (4.77 D) solvents using Lippert-Mataga method [details are outlined in supporting information S2]. Dipole moment change in the excited state of MTDCO is observed to be higher in case of protic solvents. This is according to our expectation from the fluorescence measurements of MTDCO in different homogeneous solvents. However, in the Lippert-Mataga calculation of dipole moment, only nonspecific solvent effects are considered and solvent system acting as dielectric continuum. Hence, a specific solvent effect like hydrogen bonding is thus ignored and the real picture is not represented. However, a multi-parameter approach is always preferred to estimate the influence of a particular solvent parameter on the photophysics of MTDCO. Now to measure individual contributions of different modes of solute-solvent interactions, Kamlet-Taft Solvatochromic Comparison Method (KTSCM) has been widely used [43] [details are outlined in supporting information S3]. The values obtained for MTDCO using benzene as the reference solvent are given in relation (5).

$$\overline{\nu} = 26109 - 1431\pi^{*} - 2730\alpha - 987\beta \quad (5)$$

Where, π^{*} is a measure of the polarity/polarizability effects of the solvent; α scale is an index of solvent HBD (hydrogen bond donor) acidity and β scale is an index of solvent HBA (hydrogen bond acceptor) basicity. The negative sign of the coefficients indicates the bathochromic shift of the emission maximum of MTDCO with increase in solvent polarity, ability of H-bond donor acidity and ability of H-bond acceptor basicity of the solvent respectively. The relative magnitudes of coefficients indicate that HBD acidity of the solvent plays a major role in governing the photophysics of the compound while HBA basicity of the solvent has the least contribution. Combined effects of dipolarity and polarizability of the solvent are expressed with a single parameter in Kamlet-Taft's method. However, these two effects have been separated in the modified version of Catalan method [44] [details are outlined in supporting information S4]. We have used the values of emission maxima of MTDCO from Table 1 and the values of the solvent parameters [45] from Supporting Information S1. Following values are obtained for MTDCO (Eq. 6) using benzene as the reference solvent.

$$\sigma = 26109 - 4181SA - 1795SB + 1533SP - 539SdP \quad (6)$$

Here, SA, SB, SP, SDP represent solvent acidity, solvent basicity, solvent polarizability and solvent dipolarity respectively.

From both multi-parameter methods of Kamlet-Taft and Catalan, it is apparent that acidity of the solvent plays an important role in controlling the photophysics of MTDCO. From Catalan's method, it is evident that solvent polarizablity is less significant than solvent dipolarity.

Table 3 Fluorescence lifetime of MTDCO with increasing concentration of HSA

HSA (concentration)	$(a_1)/(a_2)$	τ_1 / τ_2 (ns)	χ^2	τ_{av} (ns)
0 M	(1)/(0)	2.57	1.00	2.57
0.0000075 M	(1)/(0)	2.67	1.05	2.67
0.0000150 M	(0.23)/(0.77)	1.52/3.12	1.09	2.75
0.0000300 M	(0.24)/(0.76)	1.40/3.26	1.09	2.82
0.0000375 M	(0.21)/(0.79)	1.13/3.37	1.07	2.89
0.0000562 M	(0.21)/(0.79)	1.11/3.53	1.07	3.03
0.0001125 M	(0.26)/(0.74)	1.04/3.76	1.16	3.05

Effect of Binary Mixtures on the Excited State Affairs of MTDCO (Role of Water)

Here, we have made an attempt to study the solvation dynamics of MTDCO in dioxane-water binary mixture. Dioxane has a unique property to form small water clusters where the dynamical properties of water molecules can be monitored by changing the composition of binary mixtures [46–48]. Similar to that of homogeneous solvents, the absorption spectra of MTDCO do not change appreciably in this binary solvent mixture (Supporting Information S5). Emission profile shows appreciable change as the percentage of water increases.

It is evident from Fig. 4a-c as the concentration of water increases up to 40 %, fluorescence intensity enhancement is observed along with a systematic bathochromic shift. Further increase in water proportion indicates regular increase in

Table 4 Fluorescence lifetime of MTDCO with increasing concentration of BSA

BSA (concentration)	$(a_1)/(a_2)$	τ_1 / τ_2 (ns)	χ^2	τ_{av}
0 M	(1)/(0)	2.57	1.00	2.57
0.0000075 M	(0.18)/(0.82)	1.03/2.95	0.99	2.60
0.0000112 M	(0.22)/(0.78)	1.19/3.05	1.01	2.64
0.0000150 M	(0.26)/(0.74)	1.29/3.15	1.00	2.67
0.0000300 M	(0.31)/(0.69)	1.26/3.35	1.10	2.70
0.0000525 M	(0.30)/(0.70)	1.19/3.36	1.16	2.70
0.0000825 M	(0.29)/(0.71)	1.15/3.37	1.19	2.73
0.0000975 M	(0.34)/(0.66)	1.23/3.63	1.19	2.82
0.0001275 M	(0.37)/(0.63)	1.29/3.78	1.34	2.86
0.0001425 M	(0.45)/(0.55)	1.50/4.16	1.15	2.96

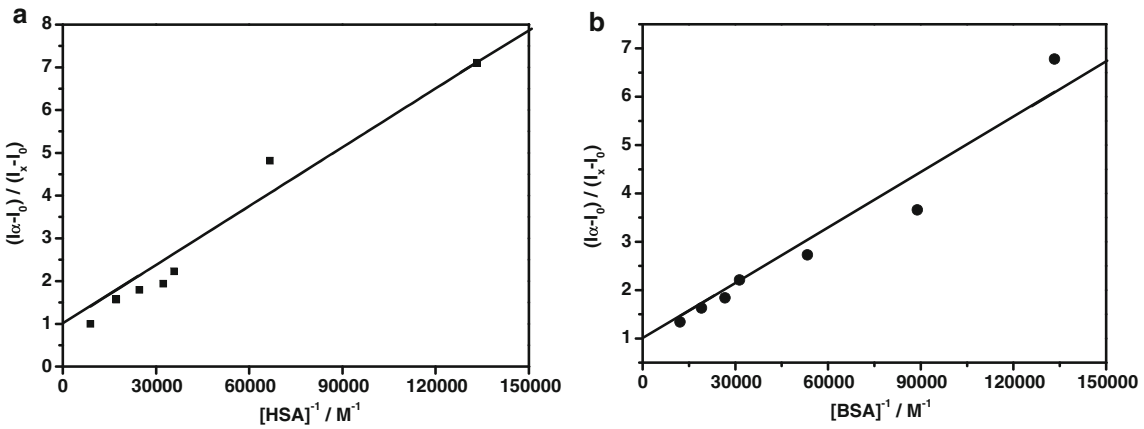

Fig. 10 Benesi– Hildebrand plot of $(I_\infty - I_0)/(I_x - I_0)$ vs. $[M]^{-1}$ for complex formation between **a** MTDCO-BSA and **b** MTDCO-HSA. Concentration of the compound is 1×10^{-6}M. The linear regression indicates a 1:1 stoichiometry

emission wavelength but fluorescence intensity decreases. Shifts in the spectral maxima are brought about by strengthening and weakening of H-bonds in the electronic excited state compared to their ground states. The spectral red-shift with increase in water proportion indicates that the intermolecular H-bonding formed with the keto-carbonyl of MTDCO is strengthened in the electronic excited state in comparison to aprotic solvents. Excited state spectral possessions of MTDCO in such binary mixture indicate the presence of two fluorescing species. One is MTDCO and the other one is h-MTDCO (hydrogen bonded). At low water proportion, MTDCO is the fundamental fluorescing species whereas, at high water proportion, emission is mainly observed from h-MTDCO. Lifetime experiment (Fig. 4d) also indicates the same conclusion as obtained from the steady state results [Corresponding decay parameters are given in Supporting Information S6]. Initially, with increase in water, lifetime increases (0.39 to 2.68 ns), followed by a certain decrease in lifetime (2.68 to 2.57 ns) as the percentage of water increases beyond 50 %. Probably, MTDCO experiences a competition between hydrogen bonding and dielectric constant. Initially, addition of water increases dielectric constant around MTDCO whereas in the latter part, hydrogen bonding interactions prevail.

Modification Observed in the Photophysical Responses of MTDCO in Presence of Surfactant and β-cyclodextrin Environments

Broad unstructured absorption band around 342 nm is observed in aqueous solution of MTDCO. On addition of surfactants like sodium dodecyl sulphate (SDS), cetyltrimethylammonium bromide (CTAB) and Triton X-100 (TX-100), nature of absorption spectra remains practically unchanged (not shown in figure). This implies that ground state is feebly sensitive to the nature of the surfactant environment. However, the fluorescence emission spectrum is

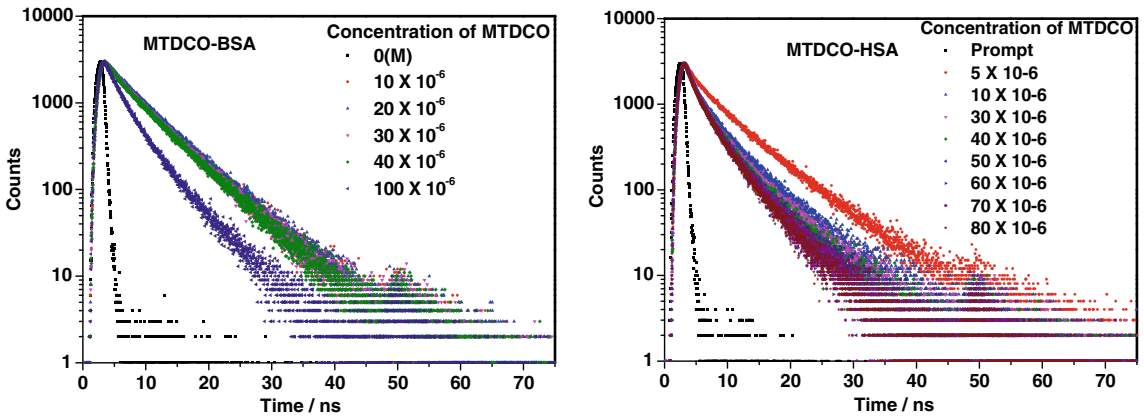

Fig. 11 Changes in fluorescence decays of BSA and HSA with increasing concentrations of MTDCO (pH=7.4 and ionic strength=0.15 M). BSA and HSA are excited using a 280 nm LED

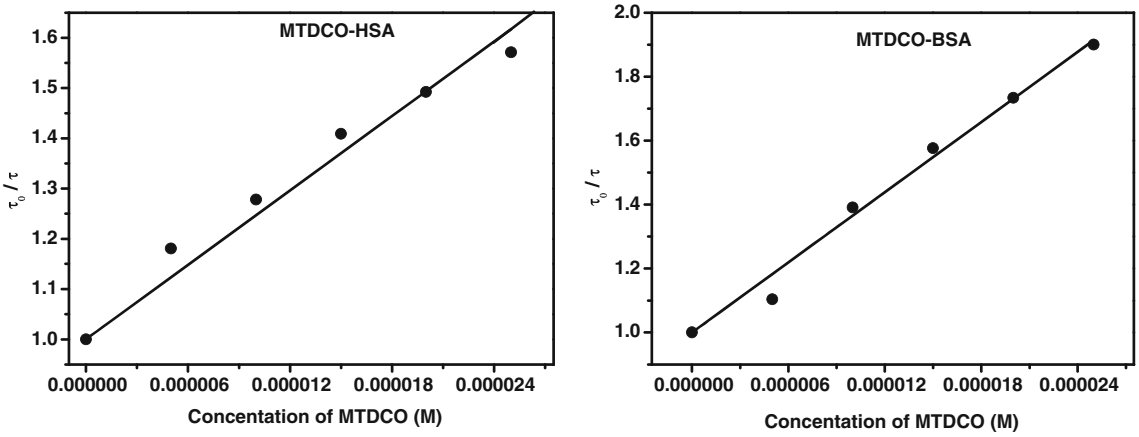

Fig. 12 Stern-Volmer plot for the quenching of HSA and BSA lifetime with MTDCO with the data obtained from Fig. 11

found to be strongly dependent on the concentration of surfactant in solution (Fig. 5.).

On gradual addition of surfactants to the aqueous solution of MTDCO (single, broad, unstructured, τ ~2.57 ns), a hypsochromic shift is observed with respect to ~467 nm depending on the nature of surfactants. This suggests that the surrounding environment of MTDCO gets modified as we move from pure aqueous to aqueous micellar environments. Significant enhancement in emission intensity is observed coupled with a hypsochromic shift and an increase in lifetime. This indicates that MTDCO resides in such an environment where the polarity is less than that of the bulk water. As we move from cationic surfactant CTAB (~33 nm) to anionic surfactant SDS (~19 nm) and then to non-ionic surfactant TX-100 (~32 nm), the degree of hypsochromic shift varies. Among all surfactants, increase in lifetime (Fig. 6) is maximum in anionic surfactant SDS (τ~2.57 to τ~2.93). On the other hand, absorption profile of MTDCO shows no significant change on increasing the concentration of aqueous β-CD (not shown in figure). Prominent changes are observed in the emission profile of MTDCO (Fig. 5d.) with increasing β-CD concentration. Significant intensity enhancement is observed coupled with a considerable blue shift of the emission maxima (from λ_{em}~467 nm to~448 nm). This observation indicates the formation of an inclusion complex between the host β-CD and the guest MTDCO molecule. Fluorescence lifetime studies (τ~2.57 to τ~3.14) (Fig. 6.) also validate the same observation obtained from the steady state result. Rigidity is imparted to the molecular framework of MTDCO when confinement is imposed by the formation of inclusion complex. Vibrational and rotational degrees of freedom are seized and there is an increase in fluorescence lifetime due to depletion of non-radiative decay channels.

Prediction of the precise location of a fluorophore within the microenvironment is an extremely important study in the viewpoint of probe-micelle interaction in order to envisage the exact location of a fluorophore within the microenvironment. It has been quite fascinating to observe whether MTDCO binds either at non-polar core formed by the hydrocarbon tails of the surfactant or at the stern layer containing the head groups or comparatively broader and disperse Gouy–Chapman layer that embraces majority of the counter ions [49, 50]. Plot of fluorescence maximum of MTDCO in water–dioxane mixtures against $E_T(30)$ of the solutions shows almost linear correlation between the two as indicated in Fig. 7.

Figure 7. thus helps to conclude micropolarity values around the probe after complete micellization to be 56.04, 51.75 and 50.64 in SDS, TX-100 and CTAB micelles, respectively. The above study indicates that in presence of different surfactants, after complete micellization, micropolarity is close to that of pure alchohol solution. Literature reports [49] also suggest that the environment in the micellar interface often resembles alcohol systems. Thus, in the present case, the fluorophore resides in the micelle-water interfacial region and does not penetrate deep into the less polar micellar core. In order to have a better vision regarding the interaction between MTDCO and the micellar units, binding constants play an influential role. We have used the fluorescence intensity data of MTDCO to determine binding constant values using the methods described by Almgren et al. [24, 51–53] (Details are outlined in Supporting Information S8) and listed in Table 2. The free energy changes for the probe–micelle

Table 5 Stern-Volmer constants for the quenching of the fluorescence lifetime of HSA and BSA with MTDCO

Protein	K_{SV} in M^{-1}
HSA	24687.32 (14856.12)
BSA	36553.51 (30764.22)

Corresponding Stern-Volmer constants obtained from the steady state experiments are within brackets

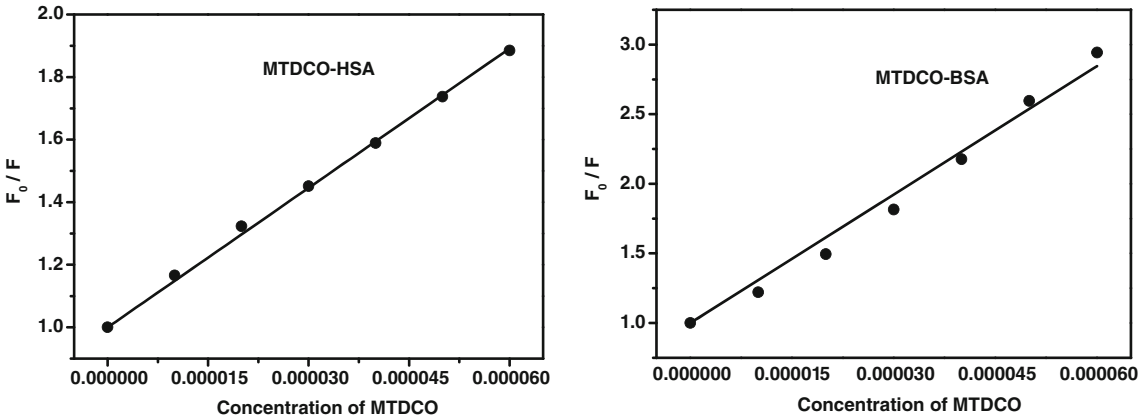

Fig. 13 Stern-Volmer plot for the quenching of HSA and BSA fluorescence with MTDCO with the data obtained from Fig. 17a and b respectively ("Fluorescence Resonance Energy Transfer from Albumin Proteins to MTDCO" section)

binding process for different micellar systems have been calculated at ambient temperature (298 K) based on the *K* values.

Literature survey indicates that the average radius of spherical micellar aggregates formed by SDS is 30 Å whereas the radius is 50 Å for TX-100 micelle [50]. In the case of cationic micellar medium formed by CTAB, radius is 22 Å [50]. From the binding constant values it is evident, MTDCO fits better in Triton-X 100 environment. Similarly, attempt has been made for a quantitative assessment of inclusion complex formation of MTDCO and β-CD to understand the stoichiometry of the complex, binding constant (K) and free energy change (ΔG) of the process. To suit this purpose, we have considered modified version of Benesi–Hildebrand plot (Eq. 7) [54] (Details are outlined in Supporting Information S9). This confirms a 1:1 stoichiometry for MTDCO:β-CD complex and at the same time permits us to calculate the extent of binding constant as K (±10 %)=1/slope=3894.854 M^{-1} which then leads to a free energy change of ΔG=−RT ln K=−20.20 kJ mol^{-1} representing the impulsiveness of the process of inclusion complex formation [25].

Interaction of MTDCO with Serum Albumins

Absorption and Fluorescence

Absorption spectrum of MTDCO in phosphate buffer (PBS, pH=7.2) shows a broad unstructured absorption band with maximum at ~340 nm. Figure 8a and b show the modifications of the absorption spectrum on subsequent addition of BSA and HSA respectively.

Gradual addition of the proteins results in a slight increase in the absorbance with no significant change in wavelength. Room temperature emission spectrum of MTDCO in phosphate buffer solution is characterized by a broad and unstructured band with a maximum at around 473 nm. On gradual addition of the proteins to the solution of MTDCO, the emission spectrum gets remarkably modified showing a radical increase in the emission yield with an associated blue shift of 25 nm in case of HSA (Fig. 9a) and 20 nm in case of BSA (Fig. 9b) respectively. The hypsochromic shift in the emission maximum of MTDCO in the protein media indicates a lowering in the polarity of the microenvironment around the

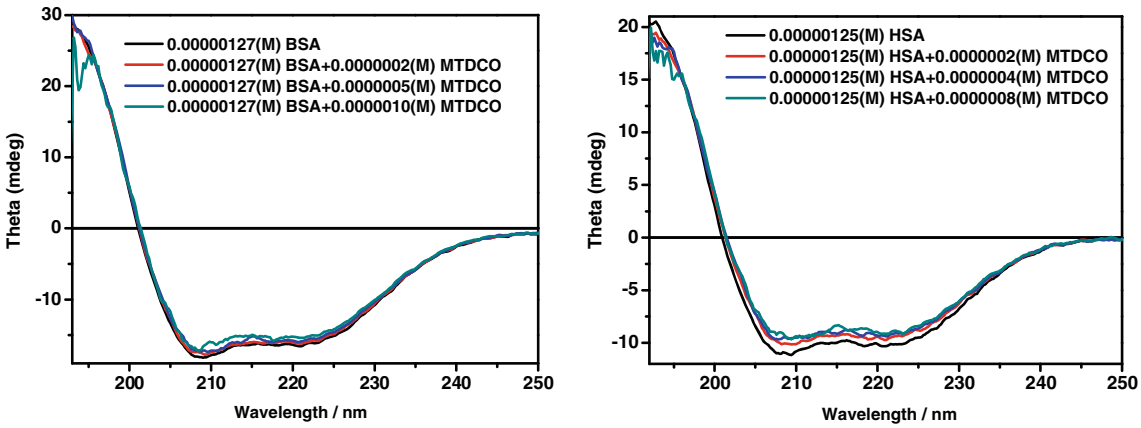

Fig. 14 Far UV CD spectra of HSA (0.00000125 M) and BSA (0.00000127 M) with addition of MTDCO

Table 6 Mean residue ellipticity (MRE) and a-helicity contents of BSA and HSA with the addition of MTDCO

Conc. MTDCO	BSA		Conc. MTDCO	HSA	
	MRE_{222nm}	% alpha helix		MRE_{222nm}	% alpha helix
0	−14870.44	56.8	0	−13883.76	53.5
0.0000002(M)	−14830.22	56.6	0.0000002(M)	−12866.49	50.2
0.0000005(M)	−14713.17	56.3	0.0000004(M)	−12479.64	48.9
0.0000010(M)	−14322.50	54.9	0.0000008(M)	−12131.53	47.7

probe. The alterations of the emission spectrum in the presence of HSA and BSA indicate that the microenvironments around the fluorophore in the protein solutions are completely different from the aqueous buffer medium and subsequently help us to infer a binding interaction (detailed discussions are mentioned in "MTDCO–protein Binding" section) between the MTDCO and the proteins.

In both the proteins, the fluorescence lifetime (Tables 3 and 4) of MTDCO increases with increase in concentration of protein (τ~2.57 to τ~3.05 in case of HSA and τ~2.57 to τ~2.96 in case of BSA). It is also evident from Tables 3 and 4 that, increase in fluorescence lifetime is higher in case of HSA compared to that in BSA. This signifies that in case of HSA, degree of motional restriction and rigidity of the microenvironment is higher. While interposing the emission maximum of MTDCO in the presence of BSA and HSA in Fig. 7, we can determine the micropolarity around the probe. In terms of $E_T(30)$ parameter, the polarity of the BSA and HSA environment is, thus, found to be 55.7 and 53.5 respectively.

MTDCO–protein Binding

The binding ability of compounds with proteins determines their usage as models of drugs and therapeutic agents [55]. With the purpose of evaluating the binding interaction between MTDCO and the albumin proteins, the binding constant values have been determined from the fluorescence data following the modified Benesi–Hildebrand equation.

$$(I_\infty - I_0)/(I_x - I_0) = 1 + (K[M])^{-1} \quad (7)$$

Where I_0, I_x and I_α are the fluorescence intensities of MTDCO considered in the absence of protein, at an intermediate protein concentration and at a concentration for complete interaction, respectively; K being the binding constant and [M] is the free protein concentration. A plot of $(I_\alpha - I_0 / I_x - I_0)$ against $[M]^{-1}$ shows linear variation justifying the validity of the Benesi–Hildebrand equation for the present case and therefore settles one-to-one stoichiometry for the probe:protein complex. The concentration of the proteins is much greater than that of MTDCO would be important to be mentioned at this juncture. Hence, the concentration of the uncomplexed or free proteins is more than that of the protein complexed with MTDCO. Evidently, therefore, the said analysis can consider the Benesi–Hildebrand equation effective in this case. At lower concentration of proteins where complexation with the compound leads to an appreciable change in the free protein concentration from the total, it is observed that the equation is not obeyed. This is deduced from the deviation from linearity in the latter portion of the plots (Fig. 10). The

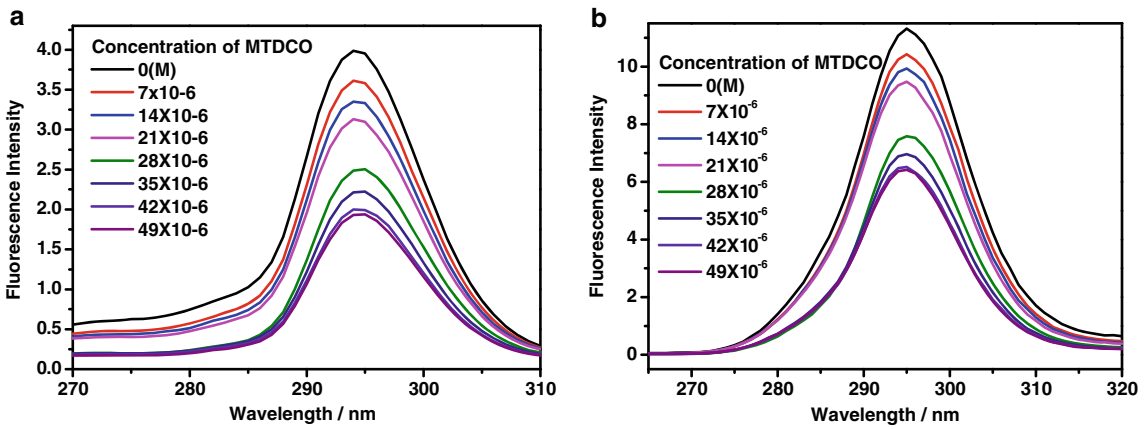

Fig. 15 Synchronous fluorescence spectra of HSA: **a** $\Delta\lambda$=60 nm; **b** $\Delta\lambda$=15 nm

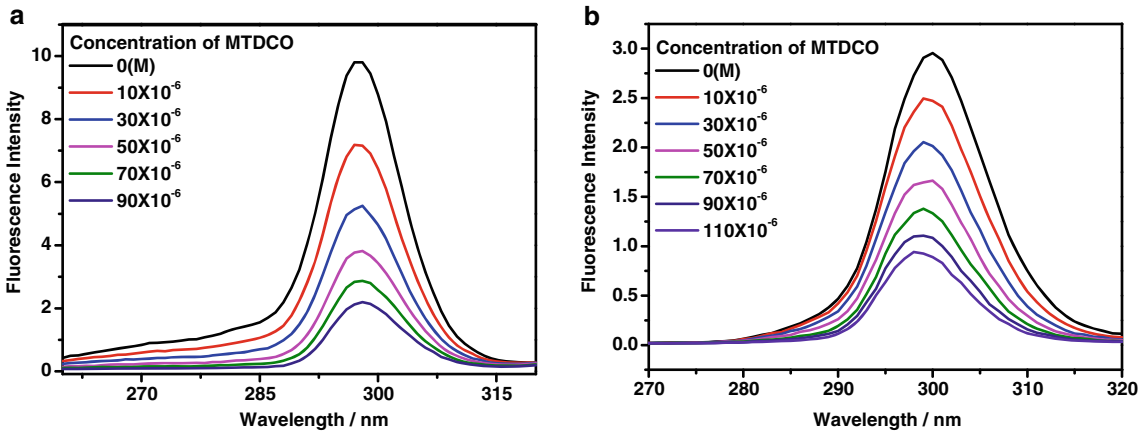

Fig. 16 Synchronous fluorescence spectra of BSA: **a** $\Delta\lambda$=60 nm; **b** $\Delta\lambda$=15 nm

values of K, thus obtained at 298 K are 26142 M^{-1} for BSA ($\Delta G=-RT \ln K=-25.20$ kJ mol^{-1}) and 21795 M^{-1} for HSA ($\Delta G=-RT \ln K=-24.75$ kJ mol^{-1}). The binding constant values are indicative of the relative stabilities of the MTDCO–protein complexes.

The obtainment of the binding interaction between MTDCO and BSA/HSA led us to see the denaturing effect of the protein on its binding activity and on the overall photophysics of the probe [56]. The present analysis has required us to use urea [57] (0 M to 6 M) and guanidine hydrochloride [58] (GuHCl, 0 M to 6 M) as the chaotropic agents to investigate the denaturing process. The emission pattern showed a behaviour that was entirely the opposite of that observed during binding of MTDCO to the proteins. A consistent red shift is observed with the addition of urea and guanindine hydrochloride alongside a decrease in the fluorescence intensity. (Detailed discussions are given in Supporting Information S10).

Perturbation in the Fluorescence Emission of Proteins on Addition of MTDCO

The attenuation of fluorescence intensity, F and lifetime, τ of the proteins on interaction with MTDCO is expressed with the following Stern-Volmer equation [59]:

$$\frac{F_0}{F} = \frac{\tau_0}{\tau} = 1 + K_{SV}[Q] \tag{8}$$

Where, K_{SV} is the Stern-Volmer quenching constant. Figure 12 represents the Stern-Volmer plot for the quenching of the fluorescence lifetime of HSA with MTDCO (data obtained from Fig. 11). Table 5 lists the corresponding Stern-Volmer constants. Corresponding Stern-Volmer plot is given in Fig. 13 for the quenching of BSA and HSA fluorescence with MTDCO with the data obtained from Fig. 17 ("Fluorescence Resonance Energy Transfer from Albumin Proteins to MTDCO" section). Linear Stern–Volmer plots

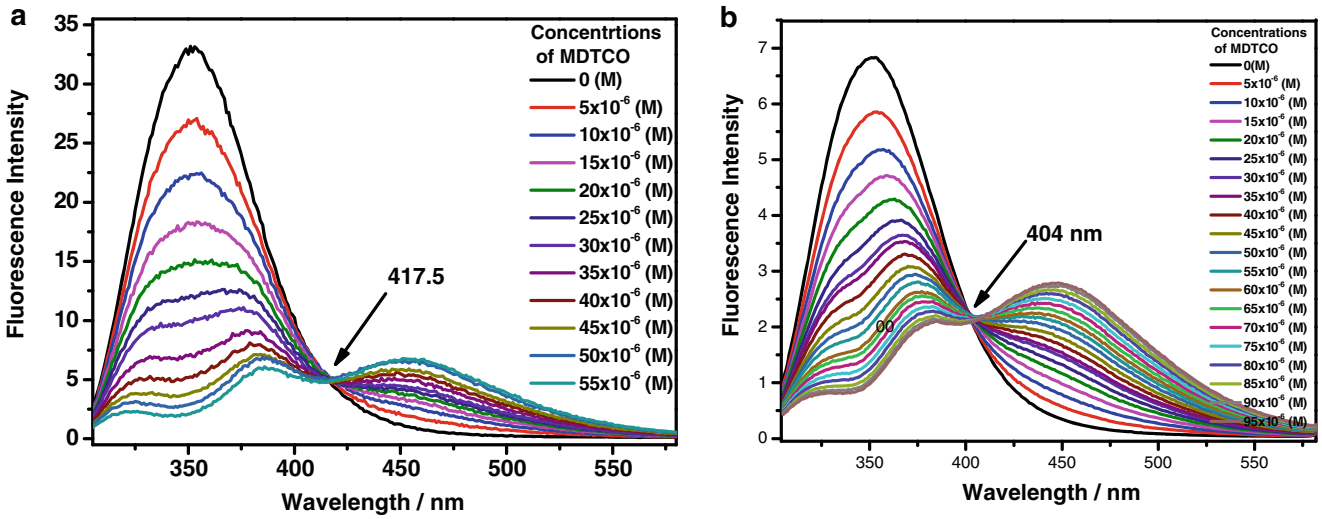

Fig. 17 Fluorescence spectra of **a** BSA and **b** HSA as a function of MTDCO concentrations (λ_{exc}=280 nm) in aqueous PBS buffer solution

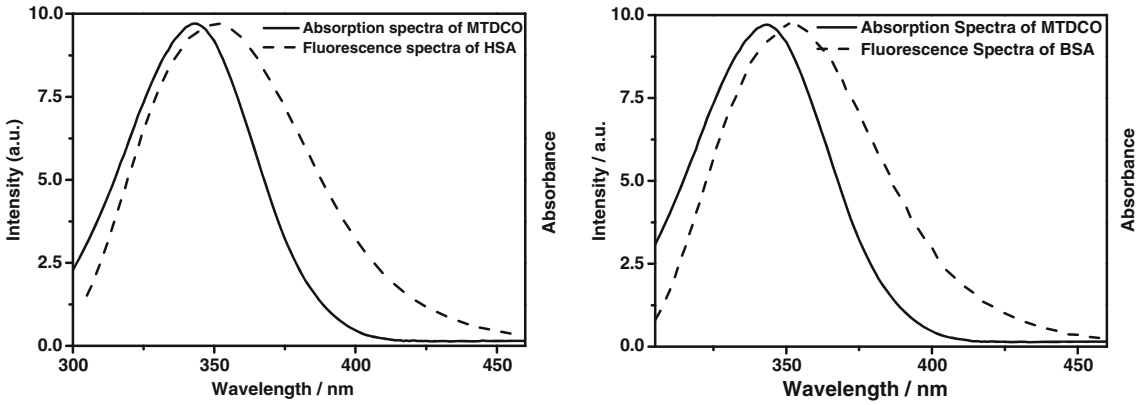

Fig. 18 Overlap of fluorescence spectrum of Protein and absorption spectrum of MTDCO

may either indicate the existence of just a binding site for MTDCO in the proximity of the tryptophan, or the existence of more than one site spatially arranged so that they are equally accessible to MTDCO [1].

Circular dichroism (CD) spectroscopy helps to study the conformational aspects of proteins upon binding with compounds [60]. Usually perturbations of the secondary and/or tertiary structure of the proteins depend on the nature of the probe. The effect of MTDCO on the structure of serum albumins has been investigated by CD spectra in far and near UV regions. The far UV CD spectra of both the proteins exhibited two negative minima at around 209 and 222 nm. This indicates the α-helical structure of the proteins. While interacting with MTDCO, decrease in the band intensities are observed without any significant shift of the peaks. This implies that MTDCO induces a decrease in the helical structure content of the proteins (Fig. 14.). For both the proteins, the percentage of α-helix was calculated using Eqs. 9 and 10 and they were found to decrease with increasing MTDCO concentration (Table 6). Destabilization of the proteins upon binding with the MTDCO is indicated by the decrease in the MRE [61]. In CD spectra of both the proteins, no appreciable change is observed in the near UV (250–360 nm) region. This indicates that in the presence of MTDCO, there is barely any perturbation in the tertiary structure of the proteins and negates any substantial conformational changes in the aromatic and peptide regions of the protein upon binding with the MTDCO [62, 63].

$$\mathrm{MRE} = \theta / 10\mathrm{nlCp} \tag{9}$$

θ is the ellipticity in millidegree, n is the number of amino acid residues (583 for BSA and 585 for HSA), l is the path length of the cell (here 0.1 cm), Cp is the protein concentration in moles dm^{-3}. Helicity content was calculated from the MRE values at 222 nm using the following equation:

$$\%\alpha\text{-}helix = [-(MRE222nm - 2340)/30300] \times 100 \tag{10}$$

Effect of MTDCO on the Conformation of Protein Using Synchronous Fluorescence Measurements

Synchronous fluorescence measurements have been carried out in order to acquire the information on the molecular environment in the vicinity of the fluorophores (Tyr and Trp) of protein [64–68]. Synchronous fluorescence spectra of HSA and BSA (Figs. 15 and 16. respectively) have been obtained by simultaneously scanning the excitation and emission monochromator maintaining $\Delta\lambda$=15 nm (Tyr exCitation) and $\Delta\lambda$=60 nm (Trp exCitation) between them [69]. Figures 15 and 16 show the effect of MTDCO on the synchronous spectrum of protein when $\Delta\lambda$=60 nm (Figs. 15a and 16a) or $\Delta\lambda$=15 nm (Figs. 15b and 16b). As it is evident, the intensity of the tryptophan and tyrosine has decreased in the presence of MTDCO but no significant shift was noticed in the signals. This indicates that the binding between MTDCO and the protein has not led to a change in the polarity of the microenvironment of the tryptophan and tyrosine residues. However, the internal packing of the protein has changed.

Fluorescence Resonance Energy Transfer from Albumin Proteins to MTDCO

When there is an interaction between the electronic states of two fluorophores in which the excitation energy is transferred from one fluorophore (donor) to another fluorophore (acceptor) without emission of a photon the resulting phenomenon is called Fluorescence Resonance Energy Transfer (FRET) [70]. FRET is used to study the structure, conformation, spatial distribution and assembly of complex proteins

Table 7 Experimentally calculated parameters for fluorescence resonance energy transfer from HSA and BSA to MTDCO

Protein	R_0 (Å)	R (Å)	E
HSA	18.1	19.78	0.37
BSA	17.4	18.24	0.33

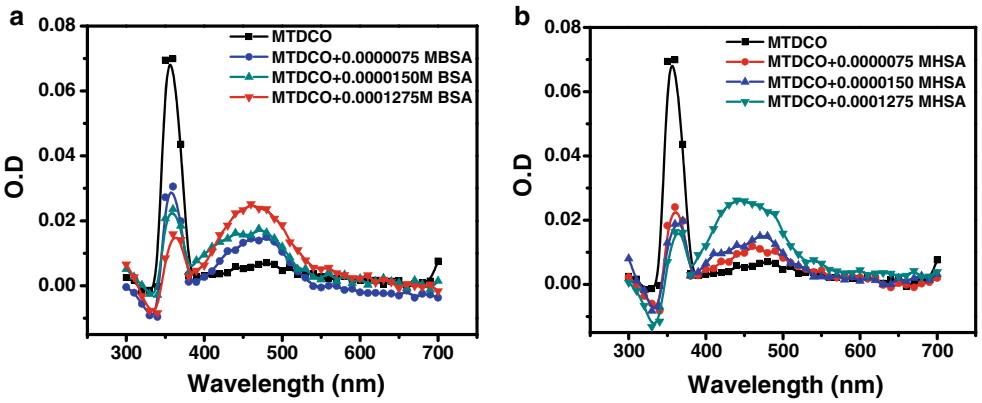

Fig. 19 Transient absorption spectra of: MTDCO (1×10^{-6}M) in aqueous PBS buffer with **a** BSA, **b** HSA 1 μs after laser flash

[71]. FRET study determines the intimacy of a guest molecule to the tryptophan moiety (intrinsic probes) in a proteinous environment. In order to locate the probable location of the probe, MTDCO, in the serum albumin environments, we have paid interest in the FRET study with the present systems. The donors (BSA and HSA) were excited at 280 nm (in the tryptophan absorption band) where the absorbance of the acceptor (MTDCO) is negligible. Fluorescence intensities of BSA and HSA (originating from the tryptophan residues) decrease on gradual addition of MTDCO, with a concomitant increase in the fluorescence intensity of MTDCO through an isoemissive point at 417.5 nm and 404 nm in case of BSA and HSA respectively (Fig. 17).

The excitation profile monitoring the emission of MTDCO shows that in the presence of BSA and HSA, besides the S_0-S_1 transition of MTDCO, a band with λ_{exc}~280 nm (corresponding to the tryptophan) appears. This provides strong evidence for the occurrence of FRET. Significant overlap between the emission spectrum of the donor BSA and HSA with the absorption spectrum of the acceptor MTDCO indicates an efficient energy transfer from the tryptophan residue present in BSA and HSA to MTDCO (Fig. 18). This is also evident that the guest molecule (MTDCO) resides close to the tryptophan moieties of the proteins [72].

Trp-212 is known to be located in a similar hydrophobic microenvironment as single Trp-214 in HSA (subdomain IIA) whereas Trp-132 is more exposed to the aqueous environment. Similarity observed in the fluorescence behaviour proves that in BSA environment the probe is located near Trp-212 rather than Trp-132. FRET parameters thus have been calculated at the same concentration of both HSA and BSA with MTDCO where there is considerable overlap of the aforesaid spectra with the aim of Förster's theory of nonradiative energy transfer. According to this theory, the efficiency of energy transfer, E has been determined from the following equation [73–76]:

$$E = 1-\left(\frac{F}{F_o}\right) = \frac{R_o^6}{R_o^6 + r^6} \tag{11}$$

Where, R_0 is the Förster distance where efficiency is just 50 % and r is the actual distance between the donor and acceptor. R_0 is calculated using the following equation:

$$R_0^6 = 8.79 \times 10^{-25}\kappa^2\eta^{-4}J(\lambda)\Phi \tag{12}$$

The value of $J(\lambda)$ has been calculated using the following formula:

$$J(\lambda) = \frac{\int F_D(\lambda)\varepsilon_A(\lambda)\lambda^4 d\lambda}{\int F_D(\lambda)d\lambda} \tag{13}$$

$F_D(\lambda)$is the fluorescence intensity of HSA (donor) at wavelength λ and $\varepsilon_A(\lambda)$ is the molar extinction coefficient of MTDCO at the same wavelength. Φ is the quantum yield of the donor HSA. η is the refractive index of the medium. κ is the orientation factor of the donor and acceptor and for random orientation of donor and acceptor a value of 2 / 3 is assumed for κ^2. The calculated values of the FRET parameters have been listed in Table 7.

Laser Flash Photolysis

In order to speculate the triplet excited state interaction between MTDCO and albumin proteins (BSA & HSA) Laser flash photolysis experiments were carried out [77–81]. Figure 19 shows the transient absorption spectra of MTDCO

Table 8 Change in lifetime at 360 nm and at 460 nm in presence of BSA

Decay	360 nm	460 nm
MTDCO	1.93±0.021 μS	1.32±0.129 μS
MTDCO+0.0000075M BSA	1.90±0.023 μS	1.87±0.063 μS
MTDCO+0.0000150M BSA	1.89±0.031 μS	1.89±0.066 μS
MTDCO+0.0001275 M BSA	1.88±0.032 μS	1.93±0.045 μS

Table 9 Change in lifetime at 360 nm and at 460 nm in presence of HSA

Decay	360 nm	460 nm
MTDCO only	1.93±0.021μS	1.36±0.061 μS
MTDCO+0.0000075M HSA	1.88±0.069 μS	1.83±0.078 μS
MTDCO+0.0000150 M HSA	1.87±0.059 μS	1.85±0.052 μS
MTDCO+0.0001275 M HSA	1.80±0.062 μS	1.89±0.061 μS

in aqueous buffer solution at 1 μs after the laser flash with maximum absorbance at 360 nm. With gradual addition of BSA/HSA, a new broad peak is observed around 460–480 nm with increase in absorbance and a gradual decrease in the peak height at 360 nm. The peak observed at 460 nm is due to the formation of radical anion of MTDCO [$MTDCO^{\cdot-}$] which indicates that a substantial amount of charge transfer occurs from albumin proteins (BSA & HSA) to MTDCO. The corresponding life time changes at 360 nm and 460 nm are given below in Tables 8 and 9. Decay profiles are given in Fig. 20.

Conclusion

The present work reports the binding interaction between a keto-tetrahydrocarbazole based fluorophore, MTDCO with surfactant, cyclodextrin and the transport proteins, BSA and HSA. The photophysical behaviour of MTDCO is modified upon interaction with all of them. This has been exploited to explore the binding efficiency and nature of the microenvironment around the probe. To the best of our knowledge this is the first report of keto-tetrahydrocarbazole based fluorophore interacting with proteins. This study suggests that MTDCO binds with both BSA and HSA. Denaturating action of urea and guanidine hydrochloride towards the albumin proteins has been demonstrated monitoring the fluorescence of MTDCO. FRET study also throws light on the location of MTDCO in the protein environments. It is proposed that the MTDCO resides close to Trp-214 in HSA and Trp-212 in BSA. Circular dichroism studies suggest that the secondary and tertiary structures of the proteins are not perturbed appreciably in the presence of MTDCO. However, the percentage of α helicity is found to decrease for both the proteins upon binding with MTDCO. Laser flash photolysis experiment indicates a

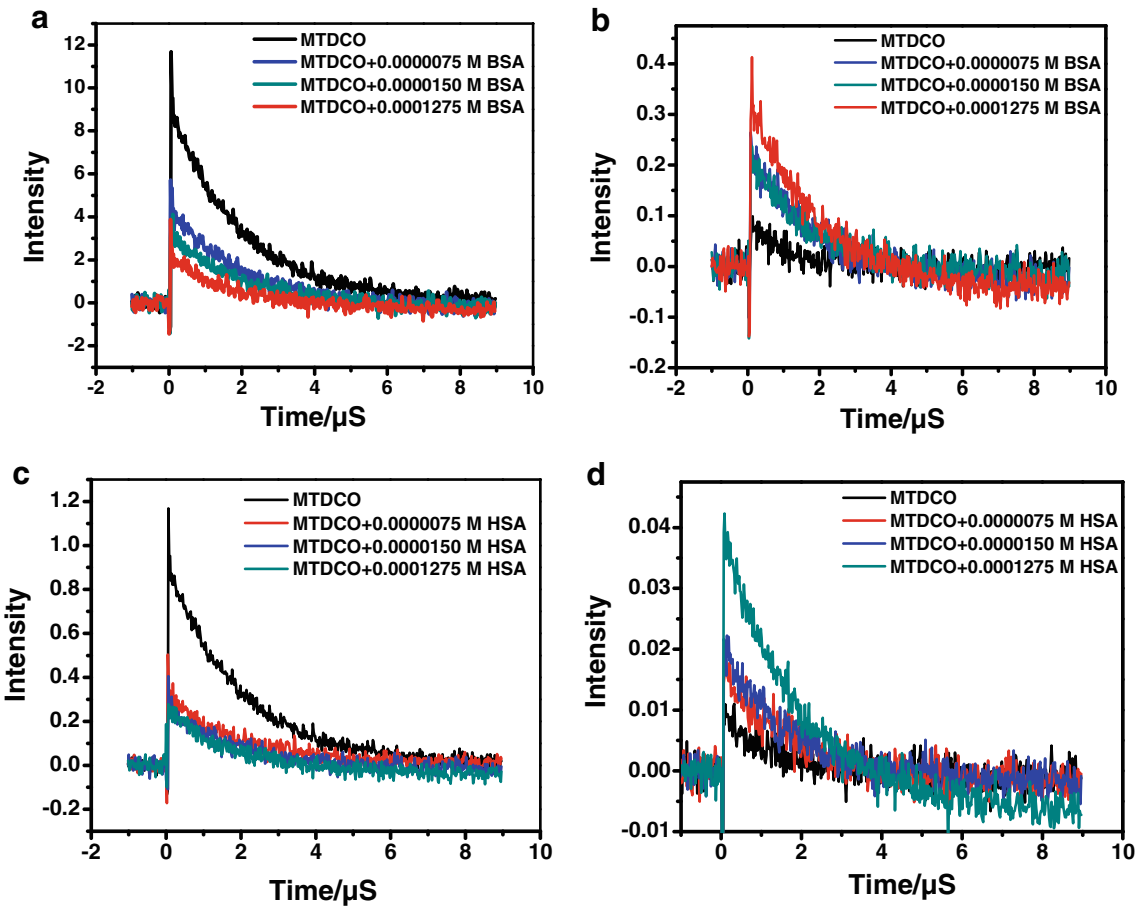

Fig. 20 Decay profile of MTDCO at various concentrations of **a** BSA at 360 nm, **b** BSA at 460 nm **c** HSA at 360 nm **d** HSA at 460 nm

considerable extent of charge transfer takes place from albumin proteins to MTDCO. Thus detection and understanding of the nature and selective binding interactions of MTDCO with serum albumins is important to establish MTDCO as a probable drug molecule.

Acknowledgments This work has been funded by Chemical and Biophysical Approaches for Understanding of Natural Processes (CBAUNP) project, SINP of the Department of Atomic Energy (DAE), Government of India. Thanks to CSIR, New Delhi for providing financial helps in the form of fellowships. We are thankful to Mrs. Sayantani Mitra for her sincere support in perusing the paper and making suitable modifications in language.

References

1. Lakowicz JR (2006) Principles of fluorescence spectroscopy, 3rd edn. Springer, New York
2. Zhang FF, Gan LL, Zhou GH (2010) Synthesis, antibacterial and antifungal activities of some carbazole derivatives. Bioorg Med Chem Lett 20:1881–1884
3. Caruso A, Lancelot JC, Kashef HE, Sinicropi MS, Legay R, Lesnard A, Rault S (2009) A rapid and versatile synthesis of novel pyrimido [5,4-*b*] carbazoles. Tetrahedron 65:10400–10405
4. Rahman MM, Gray AI (2005) A benzoisofuranone derivative and carbazole alkaloids from *Murrayakoenigii* and their antimicrobial activity. Phytochemistry 66:1601–1606
5. Knölker HJ, Fröhner W (1999) Transition metal complexes in organic synthesis, part 54. Improved total syntheses of the antibiotic alkaloids carbazomycin A and B. Tet Lett 40:6915–6918
6. Chakraborty S, Chattopadhyay G, Saha C (2011) Montmorillonite-KSF induced Fischer indole cyclization under microwave towards a facile entry to 1-keto-1,2,3,4-tetrahydrocarbazoles. Ind J Chem B 50:201–206
7. Bhattacharyya P, Biswas GK, Barua AK, Saha C, Roy IB, Chowdhury BK (1993) Clausenalene, a carbazole alkaloid from *Clausena heptaphylla*. Phytochemistry 33:248–250
8. Sohrab MH, Mazid MA, Rahman E, Hasan CM, Rashid MA (2001) Antibacterial activity of *Clausena heptaphylla*. Fitoterapia 72:547–549
9. Mitra AK, Ghosh S, Chakraborty S, Sarangi MK, Saha C, Basu S (2012) Photophysical properties of an environment sensitive fluorophore 1-keto-6,7-dimethoxy-1,2,3,4-tetrahydrocarbazole and its excited state interaction with N, N-dimethylaniline: a spectroscopic investigation. J Photochem Photobiol A 240:66–74
10. Mitra AK, Ghosh S, Chakraborty S, Basu S, Saha C (2013) Synthesis and spectroscopic exploration of carboxylic acid derivatives of 6-hydroxy-1-keto-1,2,3,4-tetrahydrocarbazole: Hydrogen bond sensitive fluorescent probes. J Lumin 143:693–703
11. Ghosh S, Mitra AK, Saha C, Basu S (2013) Tuning the solution phase photophysics of two de novo designed hydrogen bond sensitive 9-methyl-2,3,4,9-tetrahydro-1H-carbazol-1-one derivatives. J Fluoresc 23:1179–1195
12. Mitra AK, Ghosh S, Sarangi MK, Chakraborty S, Saha C, Basu S (2014) Photophysics of a solvent sensitive keto-tetrahydrocarbazole based fluorophore and its interaction with triethylamine: a spectroscopic inquest under surfactant and β-CD confinement. J Mol Str 1074:617–628
13. Mitra AK, Ghosh S, Sarangi MK, Sau A, Saha C, Basu S (2014) Influence of microheterogeneity on the solution phase photophysics of a newly synthesised, environment sensitive fluorophore 2-((7,8-dimethyl-1-oxo-2,3,4,9-tetrahydro-1H-carbazol-6-yl)oxy)acetic acid and its tagged derivative. J Photochem Photobiol A 296:66–79
14. Bag SS, Pradhan MK, Kundu R, Jana S (2013) Highly solvatochromic fluorescent naphthalimides: design, synthesis, photophysical properties and fluorescence switch-on sensing of ct-DNA. Bio Med Chem Lett 23:96–101
15. Sarangi MK, Mitra AK, Sengupta C, Ghosh S, Chakraborty S, Saha C, Basu S (2012) Hydrogen bond sensitive probe 5-Methoxy-1-keto-1,2,3,4-tetrahydro carbazole in the microheterogeneity of binary mixtures and reverse micelles. J Phys Chem C 117:2166–2174
16. Li J, He Q, Yan X (2011) Molecular assemblies of biomimetic systems. Wiley-VCH
17. Lee YS (2008) Self-assembly and Nano-technology A force balance approach. John Wiley and Sons
18. Mallick A, Mandal MC, Haldar B, Chakrabarty A, Das P, Chattopadhyay N (2006) Surfactant-induced modulation of fluorosensor activity: a simple way to maximize the sensor efficiency. J Am Chem Soc 128:3126–3127
19. Nandi N, Bhattacharyya K, Bagchi B (2000) Dielectric relaxation and solvation dynamics of water in complex chemical and biological systems. Chem Rev 100:2013–2046
20. Bagchi B (2005) Water Dynamics in the Hydration Layer around proteins and micelles. Chem Rev 105:3197–3219
21. Bhattacharyya K (2003) Solvation dynamics and proton transfer in supramolecular assemblies. Acc Chem Res 36:95–101
22. Kalyansundaram K (1987) Photochemistry in microhetrogenoussystems, Academic, orlando
23. Bales BL, Messina L, Vidal A, Peric M, Nasciment OR (1998) Precision relative aggregation number determinations of SDS micelles using a spin probe. A Model of Micelle Surface Hydration. J Phys Chem B 102:10347–10358
24. Chakrabarty D, Hazra P, Sarkar N (2003) Solvation dynamics of coumarin 480 in TritonX-100 (TX-100) and bile salt mixed micelles. J Phys Chem A 107:5887–5893
25. Bender ML, Komiyana M (1977) Cyclodextrin Chemistry. Springer, New York
26. Dodziuk H (2006) Cyclodextrins and their complexes, chemistry, analytical methods, applications. Willey, VCH, New York
27. Li S, Purdy WC (1992) Cyclodextrins and their applications in analytical chemistry. Chem Rev 92:1457–1470
28. Mueller A, O'Brien DF (2002) Supramolecular materials via polymerization of mesophases of hydrated amphiphiles. Chem Rev 102: 727–758
29. Kumar CV, Buranaprapuk A, Moyer GJ, Jockush S, Turro NJ (1998) Photochemical protease: site-specific photocleavage of hen egg lysozyme and bovine serum albumin. Proc Natl Acad Sci U S A 95:10361–10366
30. Kumar CV, Buranaprapuk A (1997) Site-specific photocleavage of proteins. Angew Chem Int Ed Engl 36:2085–2087
31. Hu Y-J, Liu Y, Xiao X-H (2009) Investigation of the interaction between berberine and human serum albumin. Biomacromolecules 10:517–521
32. Lhiaubet-Vallet V, Sarabia Z, Bosca F, Miranda MA (2004) Human serum albumin-mediated stereodifferentiation in the triplet state behavior of (*S*)- and (*R*)-Carprofen. J Am Chem Soc 126:9538–9539
33. He XM, Carter DC (1992) Atomic structure and chemistry of human serum albumin. Nature 358:209–215
34. Jimenez MC, Miranda MA, Vaya I (2005) Triplet excited states as chiral reporters for the binding of drugs to transport proteins. J Am Chem Soc 127:10134–10135
35. Szacilowski K, Macyk W, Drzewiecka-Matuszek A, Brindell M, Stochel G (2005) Bioinorganic photochemistry: frontiers and mechanisms. Chem Rev 105:2647–2694
36. Pandey RK, Constantine S, Tsuchida T, Zheng G, Medforth CJ, Aoudia M, Kozyrev AN, Rogers MAJ, Kato H, Smith KM, Dougherty TJ (1997) Synthesis, photophysical properties, *in vivo*

photosensitizing efficacy, and human serum albumin binding properties of some novel bacteriochlorins. J Med Chem 40:2770–2779
37. Patrice T (2004) Photodynamic therapy, royal society of chemistry (GB)
38. Peters T (1985) Serum albumin, advances in protein chemistry, vol 37. Academic, New York
39. Zhao GJ, Han KL (2008) Effects of hydrogen bonding on tuning photochemistry: concerted hydrogen-bond strengthening and weakening. Chem Phys Chem 9:1842–1846
40. Zhao GJ, Han KL (2007) Early time hydrogen-bonding dynamics of photoexcited coumarin 102 in hydrogen-donating solvents: theoretical study. J Phys Chem A 111:2469–2474
41. Lippert E (1957) Spektroskopische Bestimmung des Dipolmomentesaromatischer Verbindungenimerstenangeregten Singulettzustand. Berichte der Bunsengesellschaftfürphysikalische Chemie 61:962–975
42. Mataga N, Kaifu Y, Koizumi M (1956) Solvent effects upon fluorescence spectra and the dipolemoments of excited molecules. Bull Chem Soc Jpn 29:465–470
43. Kamlet MJ, Abboud JL, Taft RW (1977) The solvatochromic comparison method. 6. The.pi.* scale of solvent polarities. J Am Chem Soc 99:6027–6038
44. Catalan J (2009) Toward a generalized treatment of the solvent effect based on four empirical scales: Dipolarity (SdP, a New Scale), Polarizability (SP), Acidity (SA), and Basicity (SB) of the medium. J Phys Chem B 113:5951–5960
45. Reichardt C, Welton T (2011) Solvents and solvent effects in organic chemistry. Wiley VCH, Germany
46. Critchfield FE, Gibson JA, Hall JL (1953) Dielectric constant for the dioxane—water system from 20 to 35^0. J Am Chem Soc 75: 1991–1992
47. Geddes JA (1933) The fluidity of dioxane – water mixtures[1]. J Am Chem Soc 55:4832–4837
48. Stallard RD, Amis ES (1952) Heat of vaporization and other properties of dioxane, waterand their mixtures. J Am Chem Soc 74: 1781–1790
49. Mallick A, Haldar B, Maiti S, Chattopadhyay N (2004) Constrained photophysics of 3-acetyl-4-oxo-6,7-dihydro-12H indolo-[2,3-a] quinolizine in micellar environments: a spectrofluorometric study. J Colloid Interface Sci 278:215–223
50. Rammurthy V (1991) Photochemistry in organised and constrained media, VCH, New York
51. Almgren M, Grieser F, Thomas JK (1979) Dynamic and static aspects of solubilization of neutral arenes in ionic micellar solutions. J Am Chem Soc 101:279–291
52. Saroja G, Ramachandram B, Saha S, Samanta A (1999) The fluorescence response of a structurally modified 4-Aminophthalimide derivative covalently attached to a fatty acid in homogeneous and micellar environments. J Phys Chem B 103:2906–2911
53. Das P, Mallick A, Haldar B, Chakrabarty A, Chattopadhyay N (2006) Effect of nanocavity confinement on the rotational relaxation dynamics: 3-acetyl-4-oxo-6, 7-dihydro-12H indolo-[2, 3-a] quinolizine in micelles. J Chem Phys 125:044516(1)–044516(6)
54. Benesi HA, Hilderbrand JH (1949) A spectrophotometric investigation of the interaction of iodine with aromatic hydrocarbons. J Am Chem Soc 71:2703–2707
55. Chakrabarty A, Mallick A, Haldar B, Das P, Chattopadhyay N (2007) Binding interaction of a biological photosensitizer with serum albumins: a biophysical study. Biomacromolecules 8:920–927
56. Lapange S (1978) Physicochemical aspects of protein denaturation. Wiley, New York
57. Liepinsh E, Otting G (1994) Specificity of urea binding to proteins. J Am Chem Soc 116:9670–9674
58. Nandi PK, Robinson DR (1984) Effects of urea and guanidine hydrochloride on peptide and nonpolar groups. Biochemistry 23: 6661–6668
59. Stern O, Volmer M (1919) Über die Abklingungszeit der Fluoreszenz. Physikalische Zeitschrif 20:183–188
60. Chen YH, Yang JT, Martinez HM (1972) Determination of the secondary structures of proteins by circular dichroism and optical rotatory dispersion. Biochemistry 11:4120–4131
61. Ahmad B, Parveen S, Khan RH (2006) Effect of albumin conformation on the binding of ciprofloxacin to human serum albumin: a novel approach directly assigning binding site. Biomacromolecules 7:1350–1356
62. Sengupta B, Sengupta PK (2003) Binding of quercetin with human serum albumin: a critical spectroscopic study. Biopolymers 72: 427–434
63. Banerjee T, Singh SK, Kishore N (2006) Binding of naproxen and amitriptyline to bovine serum albumin: biophysical aspects. J Phys Chem B 110:24147–24156
64. Lloyd JBF (1971) Synchronized excitation of fluorescence emission spectra. Nature Phys Sci 231:64–65
65. Vo-Dinh T (1978) Multicomponent analysis by synchronous luminescence spectrometry. Anal Chem 50:396–401
66. Vo-Dinh T (1982) Synchronous luminescence spectroscopy: methodology and applicability. Appl Spectroscopy 36:576–581
67. Rubio S, Gomez-Hens A, Valcarcel M (1986) Analytical applications of synchronous fluorescence spectroscopy. Talanta 33: 633–640
68. Patra D, Mishra AK (2002) Recent developments in multicomponent synchronous fluorescence scan analysis. Trends Anal Chem 21:787–798
69. Miller JN (1979) Recent advances in molecular luminescence analysis. Proc Anal Div Chem Soc 16:203–208
70. Förster T (1948) Intermolecular energy migration and fluorescence. Ann Phys 2:55–75
71. Förster T (1959) 10th spiers memorial lecture. Transfer mechanisms of electronic excitation. Faraday Soc 27:7–17
72. Sengupta B, Sengupta PK (2002) The interaction of quercetin with human serum albumin: a fluorescence spectroscopic study. Biochim Biophys Res Commun 299:400–403
73. Valeur B (2002) Molecular fluorescence principles and applications, WILEY-VCH
74. Rohatgi-Mukherjee KK (2014) Fundamentals of photochemistry, 4th ed.; New Age International
75. Turro NJ (1991) Modern molecular photochemistry; University Science Books
76. Banerjee M, Maiti S, Kundu I, Chakrabarty A, Basu S (2010) Simultaneous occurrence of energy transfer and photoinduced electron transfer in interactions of hen egg white lysozyme with 4-Nitroquinoline-1-Oxide. Photochem Photobiol 86:1237–1246
77. Wang JT, Sun Q, Zhang LM, Yu SQ (2010) Solvent effects of photoinduced electron transfer reactions of triplet fluorenone with amines. Chin Sci Bull 55:2891–2895
78. Pan Y, Fu Y, Liu S, Yu H, Gao Y, GuoQ YS (2006) Studies on photoinduced H-Atom and electron transfer reactions of *o*-Naphthoquinones by laser flash photolysis. J Phys Chem A 110: 7316–7322
79. Shida T, Nosaka Y, Kato T (1978) Electronic absorption spectra of some cation radicals as compared with ultraviolet photoelectron spectra. J Phys Chem 82:695–698
80. Bixon M, Jortner (1993) Solvent relaxation dynamics and electron transfer. J Chem Phys 176:467–481
81. Barbara PF, Meyer TJ, Ratner MA (1996) Contemporary issues in electron transfer research. J Phys Chem 100:13148–13168